Realization of a Λ System with Metastable States of a Capacitively Shunted Fluxonium

N. Earnest,[1,*] S. Chakram,[1] Y. Lu,[1] N. Irons,[2] R. K. Naik,[1] N. Leung,[1] L. Ocola,[3]
D. A. Czaplewski,[3] B. Baker,[2] Jay Lawrence,[4] Jens Koch,[2] and D. I. Schuster[1,†]

[1]*The James Franck Institute and Department of Physics, University of Chicago, Chicago, Illinois 60637, USA*
[2]*Department of Physics and Astronomy, Northwestern University, Evanston, Illinois 60208, USA*
[3]*Argonne National Laboratories, Center for Nanoscale Materials, Argonne, Illinois 60439, USA*
[4]*Department of Physics, Dartmouth College, Hanover, New Hampshire 03755, USA*

We realize a Λ system in a superconducting circuit, with metastable states exhibiting lifetimes up to 8 ms. We exponentially suppress the tunneling matrix elements involved in spontaneous energy relaxation by creating a "heavy" fluxonium, realized by adding a capacitive shunt to the original circuit design. The device allows for both cavity-assisted and direct fluorescent readouts, as well as state preparation schemes akin to optical pumping. Since direct transitions between the metastable states are strongly suppressed, we utilize Raman transitions for coherent manipulation of the states.

Quantum computation with superconducting circuits has seen rapid progress over the past decade [1–3] largely due to improvements in qubit coherence [4–6]. Performing large-scale quantum computation, error correction and simulation, will require significantly longer coherence times [7,8]. Fermi's golden rule states that qubit lifetimes are governed by two factors: (1) the noise spectral density associated with environmental degrees of freedom; (2) the transition matrix elements, which are determined by the qubit wave functions. To date, improvements in superconducting qubit lifetimes have primarily been achieved by modifying the noise spectral density—for example, by filtering [9,10] and by minimizing the contributions of two-level systems [6,11]. We demonstrate a complimentary approach, making the qubit insensitive to environmental noise by reducing the transition matrix elements. This leads to qubit lifetimes as high as 8 ms, and realizes a Λ system analogous to those commonly found in atomic systems.

Most current superconducting qubit architectures are based on variants of the transmon qubit [5,12–14]. Transmons have large dipole matrix elements, simple selection rules, and a small nonlinearity, sufficient to resolve the lowest energy levels as the qubit states. In contrast, flux qubits [15–17] have a large nonlinearity, rich level structure, and selection rules that can be finely engineered to yield a smooth trade-off between decay matrix elements and gate fidelities. With the realization of a linear superinductance and the fluxonium qubit [18], this class of qubits has seen enhanced lifetimes and reduced flux-noise induced decoherence [19]. These properties make the fluxonium a promising system for engineering a Λ system.

Traditionally, a Λ system is comprised of a ground and metastable excited state, coherently coupled through a third intermediate state. Λ systems are ubiquitous in atomic physics, realized using a combination of selection rules [20], relative strengths of optical-dipole and microwave hyperfine matrix elements [21], and large differences in frequency scales in conjunction with the 3D density of states (decay rate $\gamma \propto \nu^3$) [22]. Superconducting qubits are typically not protected by symmetry-based selection rules, and possess a much smaller dynamic range of frequency scales and a 1D density of states ($\gamma \propto \nu$), making it more challenging to realize the metastability required to explore the physics associated with Λ systems. Previous work in circuit QED (CQED) has utilized the Purcell effect [23] to modify the density of states and explore multitone coherent interactions of three-level systems [24,25].

In this Letter, we present a Λ system in a capacitively shunted fluxonium circuit: the heavy fluxonium. The added capacitance further localizes the lowest energy states, exponentially suppressing the dipole matrix elements and boosting the metastable state lifetime to 8 ms. The suppressed matrix elements make controlled population transfer to this state a challenge, but we surmount this by using multitone Raman transitions in the Λ system to perform coherent operations with substantial improvement in gate fidelities relative to direct transitions.

The heavy fluxonium circuit [Figs. 1(a) and 1(b)] consists of a small-area Josephson junction connected in parallel to a capacitance (C_q) and a large superinductor (L_{JA}), realized as an array of 100 large-area Josephson junctions. To ensure idealized inductive behavior of the array, the length and individual junction size must satisfy several conditions as explained in [18]. Once these conditions are satisfied, the Hamiltonian of the fluxonium is given by

$$H_f = -4E_C \frac{d^2}{d\varphi^2} - E_J \cos(\varphi - 2\pi\Phi_{\text{ext}}/\Phi_0) + \frac{1}{2}E_L \varphi^2, \quad (1)$$
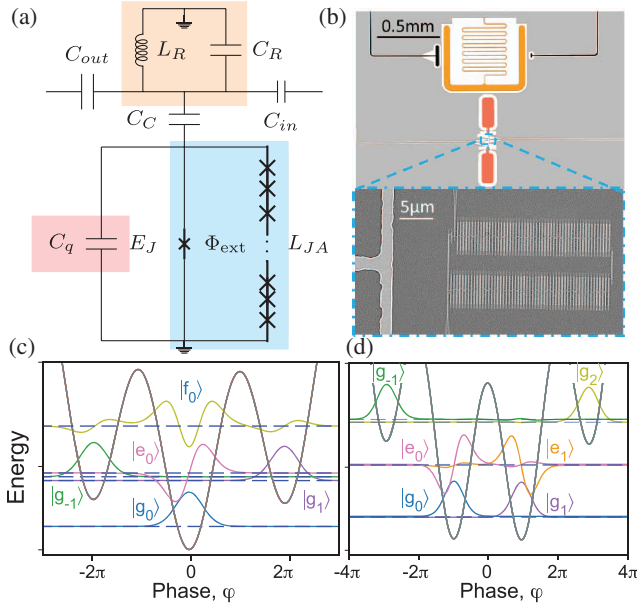
FIG. 1. (a) Equivalent circuit diagram of the heavy fluxonium capacitively coupled to a readout resonator (Supplemental Material [26]). (b) Scanning electron microscope image of the device, with a magnified view of the 100 Josephson junction array, fabricated using the bridgeless method detailed in [27]. (c) Simulated potential energy landscape or wave function at $\Phi_{ext} = 0.02\Phi_0$ demonstrating localized wave functions in three wells. (d) Simulated potential energy landscape at $\Phi_{ext} = 0.51\Phi_0$, where $|g_0\rangle$ and $|g_1\rangle$ are nearly degenerate.

where $E_C = e^2/2C_q$ is the charging energy, E_J the Josephson energy of the small junction, and $E_L = \Phi_0^2/2L_{JA}$ the inductive energy of the Josephson junction array. In contrast to earlier fluxonium devices [18], the heavy fluxonium shunts the small junction with a large capacitance [43 fF, red squares in Fig. 1(b)]. This results in a reduced $E_C/h = 0.46$ GHz, increases the effective mass of the phase degree of freedom, and produces quasilocalized states in the different wells of the potential [see Figs. 1(c) and 1(d)]. The other circuit parameters, $E_J/h = 8.11$ GHz and $E_L/h = 0.24$ GHz, are comparable to those in previous fluxonium devices. We label states by their fluxoid number $\{-1, 0, 1\}$ (number of flux quanta in the loop formed by the junctions), and by the plasmon levels within that well $\{|g\rangle, |e\rangle, |f\rangle\}$. The heavy fluxonium allows for two types of transitions: intrawell plasmons (e.g., $|g_0\rangle \leftrightarrow |e_0\rangle$), and interwell fluxons (e.g., $|g_0\rangle \leftrightarrow |g_1\rangle$).

Interwell transitions involve states with wave functions such as $\psi_{g_0}(\varphi)$ and $\psi_{g_1}(\varphi)$, which are disjoint. Accordingly, matrix elements $\int d\varphi \psi_{g_1}^*(\varphi) \hat{O} \psi_{g_0}(\varphi)$ with respect to local operators $\hat{O}(d/d\varphi, \varphi)$ will be exponentially suppressed with $\sim \exp[-\pi^2(E_J/8E_C)^{1/2}]$, inferred from considering the tails of displaced harmonic-oscillator wave functions [28]. Consequently, the $|g_1\rangle$ state of the heavy fluxonium is much longer lived relative to the original fluxonium. However, the suppressed transition matrix elements also make coherent

operations more challenging. This circuit resembles a recently reported design [29], whose dipole moment (and, thereby, the fluxon transition rate) is tunable through the use of a superconducting quantum interference device in place of a single Josephson junction. Unlike the fluxonium in [29], our heavy fluxonium—with a fixed $E_J/E_C \approx 18$—is sufficiently heavy to disallow coherent direct drives. We solve this issue by realizing a Λ system between the ground state $|g_0\rangle$, the metastable state $|g_1\rangle$, and the excited state $|f_0\rangle$, and perform coherent Raman transitions between $|g_0\rangle$ and $|g_1\rangle$.

For fast readout, the heavy fluxonium is capacitively coupled to a lossy resonator ($Q \sim 500$). The Hamiltonian of the combined system is given by [30]

$$H_S = H_f + h\nu_r \hat{a}^\dagger \hat{a} + \sum_{j,k} hg|j\rangle\langle k|\langle j|\hat{n}|k\rangle(\hat{a} + \hat{a}^\dagger), \quad (2)$$

where, $\nu_r = 4.95$ GHz is the bare frequency of the resonator and $g = 76$ MHz is the coupling between the resonator and fluxonium (as extracted from fits to spectra). $\hat{n}$ is the charge operator of the fluxonium and controls the transition rates arising from driving on the input port [C_{in} in Fig. 1(a)].

Single-tone spectroscopy (Fig. 2) reveals both the resonator photon and the plasmon transitions. The curvature of the plasmon transitions arises from flux-induced distortion of the well (Supplemental Material [26]), and allows one to easily distinguish between wells (blue and magenta lines in Fig. 2). Furthermore, the strong hybridization of the plasmon and resonator (detuned by up to 155 MHz) allows for fluorescent readout of the metastable state, over the entire
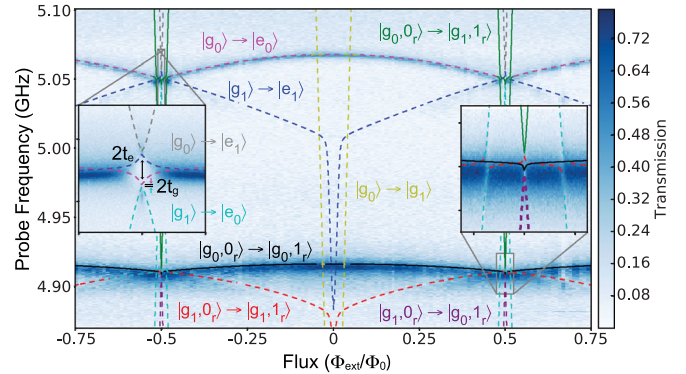

FIG. 2. Single-tone spectroscopy of the fluxonium-resonator system in the vicinity of the resonator and primary plasmon transition frequencies. Dashed lines indicate simulated energy levels of the coupled system based on device parameters extracted from fits to single and two-tone spectra. Transitions that change rapidly with flux are interwell fluxon transitions, while the flatter transitions are intrawell plasmon transitions. Left inset: interference due to coupling between the ground and excited states of neighboring wells. Right inset: features associated with fluxon transitions crossing with the resonator. The spectrum is normalized by the transmission amplitude of the bare resonator (Supplemental Material [26]).
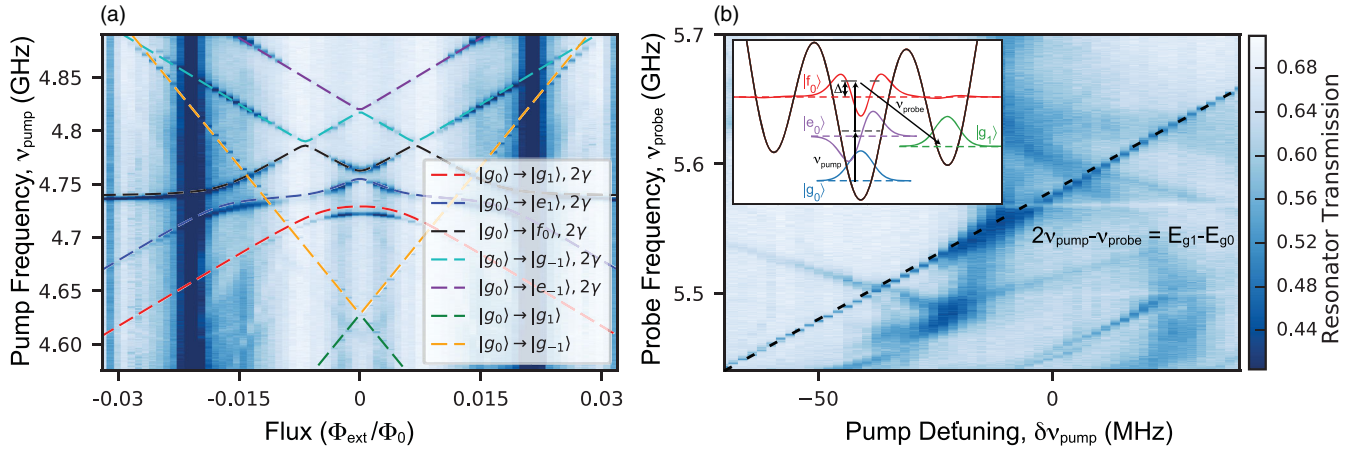
FIG. 3. (a) Two-tone spectroscopy showing direct fluxon transitions (orange and green lines) and two-photon transitions to the two-excitation manifold ($|f_0\rangle, |e_{-1}\rangle, |e_1\rangle$). State labeling for the transitions is valid for $\Phi_{\mathrm{ext}} > 0$. The $|f_0\rangle$ level serves as the intermediate state in a Λ system comprising the ground state $|g_0\rangle$ and the metastable $|g_1\rangle$ state, and assists in Raman transitions. (b) Pump-probe spectroscopy of Raman transitions between $|g_0\rangle$ and $|g_1\rangle$ as a function of pump (near $|g_0\rangle \to |f_0\rangle - 2\gamma$ transition) and probe frequency (near $|g_1\rangle \to |f_0\rangle$). The Raman transition is seen when $2\nu_{\mathrm{pump}} - \nu_{\mathrm{probe}} = E_{g_1} - E_{g_0}$, represented by the dashed line. The upper-left inset shows wave functions of the states involved in the transition. The intermediate $|f_0\rangle$ state couples to $|g_0\rangle$ via a two-photon process and has a small amplitude in the right well, with a direct dipole-allowed transition to the metastable $|g_1\rangle$ state. The dashed lines are simulated energy levels of the fluxonium-resonator system. The color bar is normalized by the transmission of the bare resonator.

flux range, through cycling the plasmon transition of the metastable state many times, similar to quantum non-demolition measurements of single trapped ions and atoms [31,32].

The tunnel splitting between the wells can be directly observed in the plasmon spectrum at $\Phi_{\mathrm{ext}} = \Phi_0/2$. At this flux location, there are two identical wells with degenerate ground and first excited states. This results in the feature shown in the left inset of Fig. 2, where the interference of the levels results in a unique rhombus-shaped avoided crossing. The separation of the level crossings forming the top and bottom corners of the rhombus (black arrows) is a direct measure of the tunnel coupling of the excited states in the well ($|e_0\rangle$ and $|e_1\rangle$), corresponding to $t_e \approx 7$ MHz. The tunnel splitting between ground states is smaller than the linewidth of the plasmon and fluxon transitions, and is inferred from the fits to be $t_g \approx 0.42$ MHz, one thousand times smaller than in previous experiments [18]. Another set of avoided crossings is visible in the resonator transmission peak (right inset of Fig. 2) at $\Phi_{\mathrm{ext}} \approx 0.5\Phi_0$. The outer set of crossings arise from the $|g_1\rangle \to |e_0\rangle$ fluxon transition (also seen in the bottom of the left inset), while the inner crossings are formed by composite resonator or fluxon transitions: $|g_1, 0_{\mathrm{res}}\rangle \to |g_0, 1_{\mathrm{res}}\rangle$ and $|g_0, 0_{\mathrm{res}}\rangle \to |g_1, 1_{\mathrm{res}}\rangle$. The latter indicate that coupling between fluxon transitions is increased when a photon is present in the resonator (Supplemental Material [26] for photon-assisted fluxon transitions). The fluxon transitions are (to first order) linear in flux, with slopes given by $\partial f / \partial \Phi_{\mathrm{ext}} \approx \pm 4\pi^2 E_L/\Phi_0 = \pm 9.59$ GHz/Φ_0.

Fluxon transitions, not seen in single-tone spectroscopy, can be identified via two-tone spectroscopy in which we monitor the transmission of the readout resonator while sweeping the frequency of a second drive tone. The lines of largest slope are the single-photon interwell fluxon transitions $|g_0\rangle \to |g_{\pm1}\rangle$. The rest of the lines are two-photon transitions to the second-excited manifold of the fluxonium-resonator system, with flat features corresponding to plasmons and sloped resonances corresponding to fluxons. Of particular importance are the two-photon features located at ~4.73 GHz corresponding to the $|g_0\rangle \to |f_0\rangle$ two-photon transition, which will assist in performing coherent operations on the qubit.

The heavy fluxonium energy-level structure allows for a variety of state-preparation schemes. We can perform T_1 measurements from the highest fluxon transition frequency of 4.65 GHz down to about 3 GHz by directly driving the fluxon transition at high powers to realize a classically mixed state (100 μs pulse duration). Below this point, we perform T_1 measurements using a process that is similar to optical pumping [33]. Through continuous cycling of the bright $|g_0\rangle \to |e_0\rangle$ plasmon in Fig. 2, we take advantage of a small probability of decaying from $|e_0\rangle$ to $|g_1\rangle$ arising from the finite matrix element between these states and incoherently "pump" the system into the $|g_1\rangle$ state, and perform a typical T_1 measurement.

Since direct fluxon transitions are forbidden, we realize faster gates by means of Raman transitions that utilize the excited levels of the fluxonium, in analogy with atomic physics. Recently, such multitone transitions have been used in superconducting qubits in the context of stabilization, and coherent population trapping [16,24,25,34–36]. As tunneling is suppressed exponentially by the depth of the well, it is

advantageous to use higher plasmon excited states. Of particular importance is the $|g_0\rangle \rightarrow |f_0\rangle$ transition shown in the inset of Fig. 3. Though the direct transition is disallowed by the symmetry of the wave functions, we can access it through a two-photon process mediated by the $|e_0\rangle$ level. Further, from the inset in Fig. 3(b), we can see that the $|f_0\rangle$ wave function has a noticeable amplitude in the right well, and $|g_1\rangle \rightarrow |f_0\rangle$ is dipole allowed. This indicates that we can use the $|g_0\rangle$, $|f_0\rangle$, and $|g_1\rangle$ states to form a Λ system. We explore Raman transitions in this Λ system by sweeping the pump and probe tone frequencies in the vicinity of these transitions, as shown in Fig. 3(b). We find a shift in the resonator transmission when $2\nu_{\text{pump}} - \nu_{\text{probe}} = E_{g_1} - E_{g_0}$, corresponding to the intended transfer of population from $|g_0\rangle \rightarrow |g_1\rangle$. The Raman transition rate is related to the Rabi rates of the two Raman tones, Ω_{probe} from $|g_1\rangle \rightarrow |f_0\rangle$, and Ω_{pump} from $|g_0\rangle \rightarrow |f_0\rangle$ according to

$$\Omega_{g_0 g_1} = \frac{\Omega_{\text{probe}} \Omega_{\text{pump}}^2}{\Delta \delta_{2\gamma}}, \tag{3}$$

where $\Delta = 2\nu_{\text{pump}} - E_{f_0} = \nu_{\text{probe}} - (E_{f_0} - E_{g_1})$ is the detuning of the pump and probe tone from the two-photon resonance, while $\delta_{2\gamma} = E_{e_0} - \nu_{\text{pump}}$ is the detuning of the two-photon $|g_0\rangle \rightarrow |f_0\rangle$ pump tone from the intermediate $|e_0\rangle$ state. Ω_{pump} and Ω_{probe} are set by the strength of the drive and by the charge matrix elements of the $|g_1\rangle \rightarrow |f_0\rangle$ and $|g_0\rangle \rightarrow |e_0\rangle$ transitions, respectively.

Having established the Λ system and the necessary tones required to perform a Raman transition between the, otherwise, forbidden metastable states, we induce Rabi oscillations by simultaneously switching on resonant pump and probe drives. The pump is detuned 30 MHz from the two-photon $|f_0\rangle$ transition, and the probe frequency is chosen to be $\nu_{\text{probe}} = 2\nu_{\text{pump}} - \Delta E_{g_1 g_0}$. At a flux value of $0.078\Phi_0$ we achieve a π pulse rate of $t_\pi \sim 400$ ns with 90% contrast [Fig. 4(b)]. While this fidelity can be further optimized in future devices, it demonstrates several orders of magnitude improvement from the direct drive which takes 100 μs to generate a classically mixed state (Supplemental Material [26]). The upper limit of the Raman transition rate arises from off-resonant excitation of the resonator through the two-photon pump drive, which drives the $|g_0, 1_{\text{res}}\rangle \rightarrow |g_1, 1_{\text{res}}\rangle$ transition.

Using these different methods, direct driving, plasmon pumping, and a three-photon Raman transition, we measure the T_1 of the device over the flux range $0 \leq |\Phi_{\text{ext}}| < 0.45\Phi_0$, as shown in Fig. 4(a). Plotting the T_1 versus flux shows improvement as we move toward $0.5\Phi_0$ and follows the (inverse square of the) charge matrix elements. This indicates that the T_1 is limited by a charge-based loss mechanism, as was also observed in the recent work on a similar fluxonium device [29]. Furthermore, we successfully measure the coherence of the fluxon transition using a standard Ramsey sequence [Fig. 4(c)] with $\pi/2$ pulses extracted from
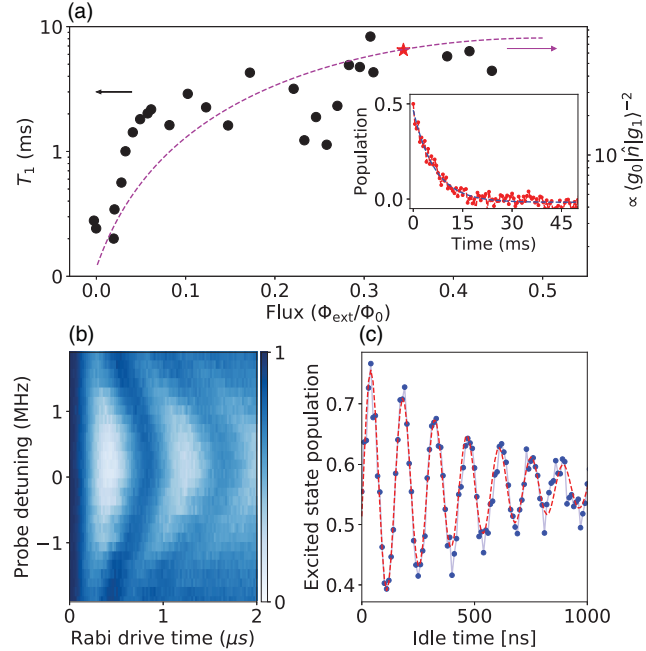

FIG. 4. (a) Energy relaxation time (T_1) as a function of magnetic flux measured through a combination of direct drive to a mixed state, plasmon pumping, and Raman transitions. The dashed purple line indicates the inverse square of the charge matrix element of the fluxon transition of interest. The inset shows the T_1 decay curve of the point indicated by the red star, after driving to a mixed state following a long Raman drive. (b) Rabi chevron obtained by detuning the probe-drive tone away from the Raman transition described in Fig. 3(b) at $\Phi_{\text{ext}} = 0.078\Phi_0$. The Raman transition is chosen to be 60 MHz from the $|f0\rangle$ level and the peak π pulse fidelity is $\sim 90\%$. (c) Ramsey experiment at $\Phi_{\text{ext}} = 0.078\Phi_0$, obtained using $\pi/2$ pulses extracted from Rabi drive of the Raman transition resulting in a T_2^* of 500–550 ns.

Rabi oscillations [Fig. 4(b)]. The T_2^* is measured to be 500–550 ns. Using the measured flux slope and assuming a $1/f$ form, this corresponds to a flux noise spectral density $S_\phi(1 \text{ Hz}) = 1.3 \ \mu\Phi_0/\sqrt{\text{Hz}}$, comparable to the flux noise measured for tunable transmons with similar magnetic shielding. This indicates that T_2^* should be improved by increasing the chain inductance, since the transition flux slope is given by $\partial f / \partial \Phi_{\text{ext}} \sim 1/L$. A spin-echo experiment using Raman transition-based $\pi/2$ and π pulses gives a $T_{2,\text{echo}}$ of 1.3 μs with a single inserted π pulse.

In summary, we have realized a heavy fluxonium in a 2D CQED architecture, with metastable states exhibiting lifetimes of several milliseconds over a broad range of flux values, likely limited by a charge-based loss mechanism. We study the coherence of the device by state preparation schemes that use the rich energy level structure of the device, including a process analogous to optical pumping. We perform coherent operations on the long-lived metastable states using a three-photon Raman transition using an excited plasmon level as the intermediate state, realizing

single-fluxon gates ($t_\pi \sim 400$ ns) that are several orders of magnitude faster than directly driving the fluxon transition with comparable microwave powers. Additionally, the relative proximity of the plasmon and readout resonator allow for photon and plasmon-mediated transitions, that could be useful for high-fidelity fluorescent readout and photon detection schemes with CQED (Supplemental Material [26]).

In future work, we seek to improve the speed and fidelity of interwell transitions, by increasing the lifetime of the plasmon states, by using more sophisticated multitone techniques [37], and by increasing the inductance to reduce dephasing rates. The fabrication techniques developed here will be useful for other types of protected qubits including the $0 - \pi$ [38] and Josephson rhombus chain qubits [39].

---

[*]nearnest@uchicago.edu
[†]david.schuster@uchicago.edu

[1] J. Kelly, R. Barends, A. Fowler, A. Megrant, E. Jeffrey, T. White, D. Sank, J. Mutus, B. Campbell, Y. Chen et al., Nature (London) 519, 66 (2015).

[2] A. Kandala, A. Mezzacapo, K. Temme, M. Takita, M. Brink, J. M. Chow, and J. M. Gambetta, Nature (London) 549, 242 (2017).

[3] N. Ofek, A. Petrenko, R. Heeres, P. Reinhold, Z. Leghtas, B. Vlastakis, Y. Liu, L. Frunzio, S. Girvin, L. Jiang et al., Nature (London) 536, 441 (2016).

[4] A. Wallraff, D. I. Schuster, A. Blais, L. Frunzio, R.-S. Huang, J. Majer, S. Kumar, S. M. Girvin, and R. J. Schoelkopf, Nature (London) 431, 162 (2004).

[5] J. Koch, T. M. Yu, J. Gambetta, A. A. Houck, D. I. Schuster, J. Majer, A. Blais, M. H. Devoret, S. M. Girvin, and R. J. Schoelkopf, Phys. Rev. A 76, 042319 (2007).

[6] H. Paik, D. I. Schuster, L. S. Bishop, G. Kirchmair, G. Catelani, A. Sears, B. Johnson, M. Reagor, L. Frunzio, L. Glazman et al., Phys. Rev. Lett. 107, 240501 (2011).

[7] A. G. Fowler, M. Mariantoni, J. M. Martinis, and A. N. Cleland, Phys. Rev. A 86, 032324 (2012).

[8] M. H. Devoret and R. J. Schoelkopf, Science 339, 1169 (2013).

[9] J. M. Martinis, M. H. Devoret, and J. Clarke, Phys. Rev. B 35, 4682 (1987).

[10] M. Reed, B. Johnson, A. Houck, L. DiCarlo, J. Chow, D. Schuster, L. Frunzio, and R. Schoelkopf, Appl. Phys. Lett. 96, 203110 (2010).

[11] J. M. Martinis and A. Megrant, arXiv:1410.5793.

[12] M. Takita, A. D. Córcoles, E. Magesan, B. Abdo, M. Brink, A. Cross, J. M. Chow, and J. M. Gambetta, Phys. Rev. Lett. 117, 210505 (2016).

[13] R. Barends, J. Kelly, A. Megrant, A. Veitia, D. Sank, E. Jeffrey, T. C. White, J. Mutus, A. G. Fowler, B. Campbell et al., Nature (London) 508, 500 (2014).

[14] R. Versluis, S. Poletto, N. Khammassi, N. Haider, D. Michalak, A. Bruno, K. Bertels, and L. DiCarlo, Phys. Rev. Applied 8, 034021 (2017).

[15] J. Mooij, T. Orlando, L. Levitov, L. Tian, C. H. Van der Wal, and S. Lloyd, Science 285, 1036 (1999).

[16] I. Chiorescu, P. Bertet, K. Semba, Y. Nakamura, C. Harmans, and J. Mooij, Nature (London) 431, 159 (2004).

[17] Z. Zhou, S.-I. Chu, and S. Han, Phys. Rev. B 70, 094513 (2004).

[18] V. E. Manucharyan, J. Koch, L. I. Glazman, and M. H. Devoret, Science 326, 113 (2009).

[19] I.-M. Pop, B. Douçot, L. Ioffe, I. Protopopov, F. Lecocq, I. Matei, O. Buisson, and W. Guichard, Phys. Rev. B 85, 094503 (2012).

[20] T. Nicholson, S. Campbell, R. Hutson, G. Marti, B. Bloom, R. McNally, W. Zhang, M. Barrett, M. Safronova, G. Strouse et al., Nat. Commun. 6, 6896 (2015).

[21] C. Monroe, D. M. Meekhof, B. E. King, W. M. Itano, and D. J. Wineland, Phys. Rev. Lett. 75, 4714 (1995).

[22] V. F. Weisskopf and E. P. Wigner, Z. Phys. 63, 54 (1930).

[23] A. Houck, J. Schreier, B. Johnson, J. Chow, J. Koch, J. Gambetta, D. Schuster, L. Frunzio, M. Devoret, S. Girvin et al., Phys. Rev. Lett. 101, 080502 (2008).

[24] S. Novikov, T. Sweeney, J. Robinson, S. Premaratne, B. Suri, F. Wellstood, and B. Palmer, Nat. Phys. 12, 75 (2016).

[25] A. A. Abdumalikov, Jr., O. Astafiev, A. M. Zagoskin, Y. A. Pashkin, Y. Nakamura, and J. S. Tsai, Phys. Rev. Lett. 104, 193601 (2010).

[26] See Supplemental Material at http://link.aps.org/supplemental/10.1103/PhysRevLett.120.150504 for details on the circuit diagram, measurement setup, direct drive rabi attempt, photon/plasmon assisted transitions, plasmon dispersion, measurement of a negative temperature state, and details on resonator/qubit hybridization.

[27] F. Lecocq, I. M. Pop, Z. Peng, I. Matei, T. Crozes, T. Fournier, C. Naud, W. Guichard, and O. Buisson, Nanotechnology 22, 315302 (2011).

[28] G. Zhu and J. Koch, Phys. Rev. B 87, 144518 (2013).

[29] Y.-H. Lin, L. B. Nguyen, N. Grabon, J. S. Miguel, N. Pankratova, and V. E. Manucharyan, preceding Letter, Phys. Rev. Lett. 120, 150503 (2018)..

[30] G. Zhu, D. G. Ferguson, V. E. Manucharyan, and J. Koch, Phys. Rev. B 87, 024510 (2013).

[31] W. Neuhauser, M. Hohenstatt, P. E. Toschek, and H. Dehmelt, Phys. Rev. A 22, 1137 (1980).

[32] N. Schlosser, G. Reymond, I. Protsenko, and P. Grangier, Nature (London) 411, 1024 (2001).

[33] C. Cohen-Tannoudji and A. Kastler, Prog. Opt. **5,** 1 (1966).

[34] E. Arimondo, Prog. Opt. **35,** 257 (1996).

[35] Y. Lu, S. Chakram, N. Leung, N. Earnest, R. K. Naik, Z. Huang, P. Groszkowski, E. Kapit, J. Koch, and D. I. Schuster, Phys. Rev. Lett. **119,** 150502 (2017).

[36] W. R. Kelly, Z. Dutton, J. Schlafer, B. Mookerji, T. A. Ohki, J. S. Kline, and D. P. Pappas, Phys. Rev. Lett. **104,** 163601 (2010).

[37] B. B. Zhou, A. Baksic, H. Ribeiro, C. G. Yale, F. J. Heremans, P. C. Jerger, A. Auer, G. Burkard, A. A. Clerk, and D. D. Awschalom, Nat. Phys. **13,** 330 (2017).

[38] J. M. Dempster, B. Fu, D. G. Ferguson, D. I. Schuster, and J. Koch, Phys. Rev. B **90,** 094518 (2014).

[39] M. T. Bell, J. Paramanandam, L. B. Ioffe, and M. E. Gershenson, Phys. Rev. Lett. **112,** 167001 (2014).